Astron. Astrophys. 345, 778–786 (1999)

ASTRONOMY
AND
ASTROPHYSICS

High resolution radio observations of NGC 4631: probing the central starburst

Götz Golla[1,2]

[1] Department of Astronomy, University of Toronto, 60 St.George Street, Toronto, Canada M5S 1A7
[2] Astronomisches Institut der Ruhr-Universität Bochum, Universitätsstrasse 150/NA 7, D-44780 Bochum, Germany

Received 13 December 1996 / Accepted 12 March 1999

Abstract. We present high resolution radio continuum observations of the edge-on galaxy NGC 4631 with the Very Large Array A, BnA & B arrays in the L–, C–, and X–band. The observed emission is limited to the inner rigidly rotating and star forming 4 kpc-diameter disk of NGC 4631. Due to missing large-scale emission of the interferometric observations we detected only 7% and 12% of the total flux densities at L– and C–band, respectively. The spectral index of the detected emission between L– and C–band is 0.23 ($S_\nu \propto \nu^{-\alpha}$), implying a thermal fraction of ∼50%. We interpret this high thermal fraction as caused by the missing large-scale emission. The non-thermal radio emission has a more extended and diffuse distribution to which our observations are not sensitive.

The emission is distributed asymmetrically with respect to the major axis, the dynamical center and the center of the stellar bulge. Gravitational interaction may play a rôle causing these asymmetries. We observe no correlation of our radio data with Hα data, and argue that this is likely caused by massive dust extinction towards the central region at optical wavelengths.

Point sources are identified at resolutions of 1.45″ and 0.83″ x 0.61″ in the central region, and their flux densities and spectral indices are derived. Two non-thermal point source complexes show strong morphological evidence for being external to NGC 4631; they are likely radio galaxies in the background. Alternatively, we discuss whether one of these sources may be the weakly active nucleus with jet–like features. Only 2–3 other point sources are non–thermal. They may be identified with supernova remnants. Using CAS A as a 'standard candle', we estimate a supernova rate of 0.009 yr^{-1}.

We estimate the thermal fraction of the total C-band radio emission of NGC 4631 with various methods, and find a likely range $f_{th} \sim$ 8–15%. Assuming a standard IMF, the thermal fraction can be translated to a high-mass ($M \gtrsim 10\,M_\odot$) star formation rate of $\sim$0.45–0.85 $M_\odot\,yr^{-1}$, and a supernova rate of 0.03–0.056 yr^{-1}. This rate is too high by a factor of three to six compared to the supernova rate estimated from the non-thermal point source population. It is shown that, in contrast to NGC 4631, the supernova and star formation rates in M 82 derived with the same methods agree well. Implications of the discrepancy, including an IMF biased toward massive stars and lower average SNR luminosities in NGC 4631 are discussed.

Key words: galaxies: individual: NGC 4631 – galaxies: ISM – galaxies: spiral – galaxies: stellar content

1. Introduction

Probing the central regions of edge-on spiral galaxies at radio wavelengths is an interesting task. Often star formation is enhanced in the central rigidly rotating disk. Dust blocks our vision at optical wavelengths. At shorter radio wavelengths we expect to see synchrotron emission from supernovae and their remnants, as well as thermal free-free emission from ionized gas. Both components are indicators of the star formation activity, and can be identified through the spectral index of the radiation.

High resolution radio imaging of the central regions of starburst galaxies in many cases has discerned a population of 'compact' radio sources. Kronberg & Wilkinson (1975) already found such compact sources in the archetypal starburst galaxy M 82 and tentatively identified them as supernova remnants (SNRs). To date more than 40 compact radio sources are identified in M 82 (Kronberg et al. 1985). Many of them were recently resolved with the MERLIN interferometer, and their nature was verified as very young supernova remnants a few pc in diameter (Muxlow et al. 1994). Most of these sources have non-thermal spectral indices $\alpha > 0.5$ ($S_\nu \propto \nu^{-\alpha}$). Their luminosities are much higher than that of the galactic SNR CAS A (7×10^{24} erg s^{-1} Hz^{-1} in C–band; van Buren & Greenhouse 1994, hereafter vBG).

In some other galaxies similar detections have been made. In NGC253 Antonucci & Ulvestad (1988) found about 35 sources with diameters not greater than 2–5 pc. Due to their small sizes these sources are likely to be young SNRs. Another population of compact sources (linear resolution limit ∼20 pc) was discovered by Duric & Dittmar (1988) in NGC 4736. Here about half of the 19 sources have thermal spectra and can be identified with optical HII-regions. Saikia et al. (1990) report on radio continuum observations of NGC 1808, and found a family of radio sources of diameters < 80 pc. They were not able to derive spectral indices of the sources so that the nature of the sources must remain unclear.

In this paper a high angular resolution study of the central radio emission of NGC 4631, including the point source popula-

Table 1. Parameters of the observations

Observing date	17 Mar	23 Aug 1994	28 Jul	16 Sep 1995
Array Configuration	A	B	A	BnA
Observing frequency (MHz)	1406	4860	4860	8440
Bandwidth (MHz)	2 x 12.5	2 x 25	2 x 25	2 x 50
Phase centre RA		$12^{\rm h}39^{\rm m}47^{\rm s}$	$12^{\rm h}39^{\rm m}42^{\rm s}$	$12^{\rm h}39^{\rm m}41.2^{\rm s}$
DEC (1950.0)		$32^\circ\ 50'$	$32^\circ\ 50'$	$32^\circ\ 49'$
Net observing time (h)	3.72	3.89	8.06	4.04
Amplitude calibrator		3C286	3C286	
Phase calibrator		1225+368	1225+368	1219+285

Table 2. parameters of the map production runs with MX/IMAGR

Band	L	C	X	C	X	C	C
Array(s)	A	B	BnA	A & B	BnA	A & B	A & B
Restoring beam width		$1.45''$		$0.83'' \times 0.61''$		$0.46'' \times 0.44''$	$0.35''$
Robustness parameter	–	–	3	0	2	0	-2
Spacing value							
of 30% taper (kλ)	150 x 120	140	150	–	–	–	–
of cutoff (kλ)	175	175	200	–	–	–	–
Convolved with CONVL	–	–	–	x	–	–	–
rms noise in TP (μJy/b)	28	15	23	15	13	19	25

tion, is presented. In Sect. 2 we describe the radio observations and the reduction of the data. In Sect. 3 various maps of the central region of NGC 4631 are shown at resolutions ranging from $1.45''$ to $0.35''$. We also give a list of identified point sources and their parameters. In Sect. 4 our results are discussed. We argue that most of the compact or slightly resolved sources are of thermal origin and discuss the distribution and morphology of this emission. We also derive a central star formation and supernova rate, discuss the nature of two peculiar sources, and identify a candidate nucleus of NGC 4631.

Through the paper we assume a distance to NGC 4631 of 7.5 Mpc, consistent with previous publications on the radio emission of NGC 4631. One arcsecond then corresponds to ~ 37 pc. Further, we adhere to a nomenclature for sources within NGC 4631 first introduced by Kronberg & Wilkinson (1975) for M 82; we give the coordinates for the equinox 1950.0, but without the hour of right ascension and the degrees in declination.

2. Observations and data reduction

We observed NGC 4631 with the Very Large Array (VLA) of the National Radio Astronomy Observatory (NRAO)[1] in its A–configuration at 1.49 GHz (L-band) and 4.86 GHz (C-band), in its B–configuration at 4.86 GHz, and in the BnA configuration at 8.44 GHz (X-band). The relevant parameters of the observations are listed in Table 1. The phase centre of the L- and C-band observations was chosen to be north–east of the centre of NGC 4631 with the specific aim of studying the spur structure in the north–eastern halo. The X-band observation was carried out in the combined BnA array because no time slot for B-array was available.

The visibility data were edited, calibrated and further processed using the 'AIPS' software package. The C–band A and B array data were shifted to the same phase center with the task 'UVFIX', and combined in the uv–plane with 'DBCON'. Parameters of the Fourier transform and map making process are given in Table 2. For the older low resolution data we used the AIPS imaging task 'MX'. In order to obtain a beam width of $1.45''$ the data were Fourier transformed applying a Gaussian weighing function to the visibilities (taper) and a cutoff at the largest spacings. Higher resolution images at various resolutions were produced with the 'AIPS' task 'IMAGR' utilizing selected values of Briggs' robustness parameter (Briggs 1995). In all maps the sidelobes of the synthesized beam were removed in the map making process, and the 'clean' components were restored with final Gaussian beams of FWHMs given in Table 2.

To facilitate spectral index studies two sets of maps were compiled, one with $1.45''$, and one with $0.83''$ x $0.61''$ beamwidth. The latter is the smallest common resolution of the BnA X–band and the combined A&B–array data, mainly determined by the elliptical BnA beam. For those maps a search and fitting of point sources was carried out with an algorithm of the NOD2[2] software package. Maps at two other higher resolutions (cf. Table 2) were produced purely for imaging purposes. The rms-noise obtained in all the maps is given in Table 2 as well.

3. Results

In the following we will discuss the radio emission of the central region based on the $1.45''$ resolution data, and then individual regions with higher resolutions down to $0.35''$. In particular, the point source population and spectral indices will be addressed.

[1] The NRAO is operated by Associated Universities Inc., under cooperative agreement with the National Science Foundation

[2] Haslam et al. 1974

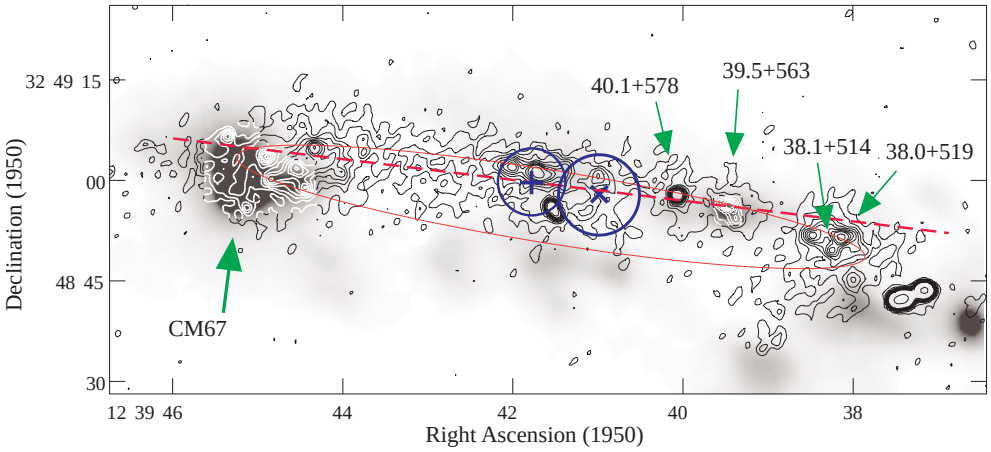

Fig. 1. 1.41 GHz radio continuum map of the central region of NGC 4631, angular resolution is 1.45″ (53 pc), contour levels are −2, 1, 2,..., 8, 10, 40, 160, 640 × 70 μJy/beam. the dashed line represents the major axis, 'x' and '+' denote the dynamical and NIR centers including the error uncertainties, the dashed-dotted ellipse is explained in Sect. 4.1. The grey-scales represent the Hα distribution from Golla et al. (1996). Names of point sources not marked in the following detailed maps are indicated.

3.1. Arcsecond-scale morphology of the central region

In Fig. 1 we present as contours the 1.4 GHz A-array radio continuum map, giving an overview over the morphology of the central radio emission of NGC 4631. The map's angular resolution of 1.45″ corresponds to a linear resolution of 53 pc. Due to the lack of sensitivity to large scale emission, the map primarily shows point-like sources and extended emission on scales less then 40″. Most of the point sources are resolved in the higher resolution maps. With the exception of a radio galaxy about 10′ south of the plane no sources were detected outside the map area shown. The corresponding 4.9 GHz B-array map is very similar so that we refrain from showing it here.

We derived flux densities of some of the point-like sources in the two 1.45″ resolution datasets. This allowed us to calculate spectral indices of compact sources, as well as emission regions resolved in the higher resolution maps. The data are listed in Table 3 and discussed in more detail below. The table also lists flux densities and spectral indices determined at higher resolutions.

Overlaid on the contours of the 1.4 GHz map in Fig. 1 is a grey-scale representation of the central Hα emission distribution from Golla et al. (1996). The near-infrared center (Aaronson 1978) and the dynamical center (Golla & Wielebinski 1994) of NGC 4631 are marked as '+' and 'x', respectively. The circles around these positions denote the rms positional uncertainty of 10″, and the HPBW of 12″, respectively, of these observations. Names of the point sources not marked in the following detailed maps are also indicated.

It appears that there is no correlation between the radio and Hα emission distributions. In particular, the bright HII region complex CM67 (cf. Fig. 1) has no distinct counterpart at radio wavelengths. There is a bright radio emitting region west of CM67 partly coincident with a western 'extension' of CM67. This may be a chance coincidence. Most of the remaining radio sources are located more in the northern parts of the Hα distribution above a central east-west going dust lane. There is only one clear coincidence of a radio and optical source: 39.5+563 (cf. Fig. 1). The general lack of correlation, as opposed to the relatively good radio–Hα correlation on larger scales in the outer disk (cf. Fig. 2 in Golla & Hummel 1994) is remarkable, and will be further discussed in Sect. 4.4.

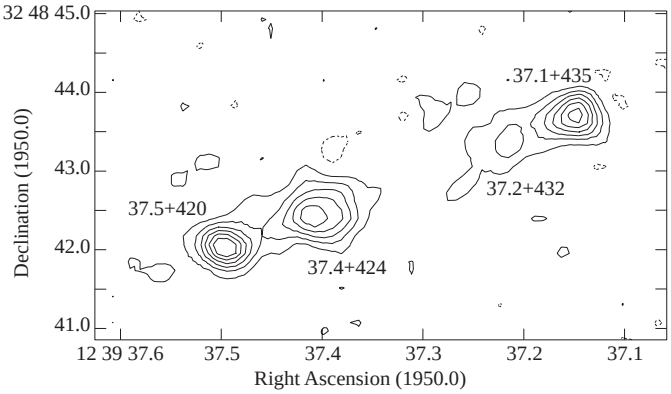

Fig. 2. Close-up view of the possible background radio galaxy at 4.86 GHz with the combined VLA A&B-array. Contours are at −2, 2, 5, 8,..., 17 × 25 μJy/beam

3.2. Sub-arcsecond scale imaging of individual emission regions

Considerably more detail is revealed in the sub-arcsecond resolution maps. Throughout the central region we find extended and filamentary radio emission superposed on more compact sources. In particular, many of the sources point-like at 1.45″ resolution are completely resolved into compact sources and/or diffuse emission. In Figs. 2 – 4 we present sub-arcsecond resolution maps of several regions within the central region.

Fig. 2 shows a close-up view of the two brightest point-like sources in the map at 0.35″ resolution in C-band. Each of the two sources is double again, and the whole set is very well aligned. The inner two sources (37.2+432 & 37.4+424) are slightly extended, whereas the outer ones (37.1+435 & 37.5+420) are unresolved.

In Fig. 3 we show the very central parts of NGC 4631 at an angular resolution of 0.46″x 0.44″. The circle and 'x' denote the positions of the NIR and dynamical centers. No source corresponds to these positions. The most interesting feature of the map is a triple source south of the NIR center, located in the center of the torus discussed in Sect. 4.1. The three sources (41.5+548, 41.5+555 & 41.6+563) are unresolved and very well aligned with a position angle of 32°.

Table 3. Flux densities and spectral indices of unresolved sources

Source ID 1950.0	category	low resolution Flux Density (μJy) L	low resolution Flux Density (μJy) C	low resolution Spectral Index α ($I_\nu \propto \nu^{-\alpha}$)	high resolution Flux Density (μJy) C	high resolution Flux Density (μJy) X	high resolution Spectral Index α ($I_\nu \propto \nu^{-\alpha}$)
37.1+435	p	–	–	–	729	554	0.50±0.05
37.2+432	m	–	–	–	145	108	0.54±0.29
37.4+424	m	–	–	–	778	569	0.58±0.05
37.5+420	p	–	–	–	615	480	0.46±0.06
38.0+519	m	–	–	–	134	159	-0.3±0.25
38.1+514	e	523	513	0.01±0.05	198	257	-0.48±0.16
39.5+563	pe	498	390	0.20±0.05	140	120	0.28±0.28
40.1+578	p	1095	521	0.61±0.03	365	324	0.22±0.10
41.0+603	e	250	207	0.03±0.12	–	–	–
41.5+548	p	–	–	–	161	135	0.32±0.25
41.5+555	p	–	–	–	160	181	-0.22±0.21
41.6+563	p	–	–	–	344	289	0.32±0.11
41.7+611	e	615	432	0.30±0.04	–	–	–
42.0+620	e	457	327	0.28±0.06	–	–	–
44.0+613	e	196	134	0.31±0.15	–	–	–
44.4+653	pe	411	245	0.44±0.07	142	85	0.94±0.34
44.4+587	pe	309	226	0.26±0.09	121	174	-0.66±0.26
44.5+617	e	373	333	0.09±0.07	68	71	-0.08±0.52
44.9+600	e	297	284	0.04±0.09	80	131	-0.91±0.38
44.9+637	e	375	404	-0.06±0.06	106	123	-0.27±0.32

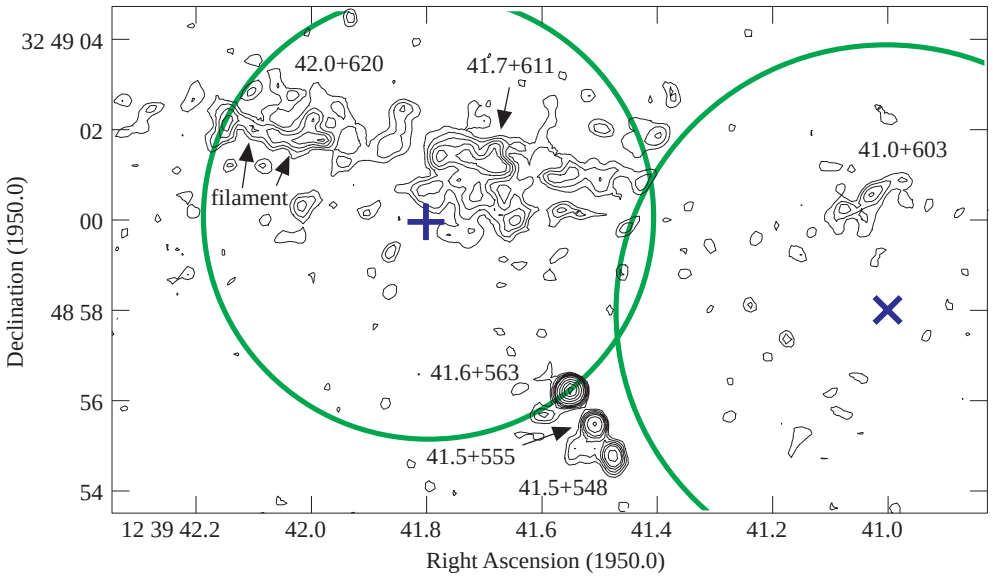

Fig. 3. Close-up view of the center of NGC 4631 at 4.86 GHz with the combined VLA A&B-array, contours are −3, 3, 4, 5, 6, 7, 9, 11, … 21 × 20 μJy/beam. The '+' and 'x' denote the near-infrared and dynamical centers of NGC 4631, respectively, and are surrounded by the corresponding positional error ellipses

The eastern-most emission region is depicted as a contour plot in Fig. 4. As opposed to earlier low-resolution work (e.g., Roy et al. 1991), this region now appears unrelated to the optically bright giant HII region complex CM67 (cf. Fig. 1). Its emission is fragmented and filamentary with no coherent features longer than about 2″ (70 pc). 6 brighter more compact sources (from 44.0+613 downwards in Table 3) are overlayed on the diffuse emission.

3.3. The list of point sources

Table 3 lists the compact sources unambiguously identified in the maps, together with their flux densities in the L & C bands as derived from the 1.45″ resolution data, and the flux densities in the C & X bands derived from 0.83×0.61″ resolution data. The flux densities were derived with the Gaussian fitting algorithm of the NOD2 software package. A twisted baselevel was subtracted prior to the fits, and the results were carefully checked by examining the residual maps.

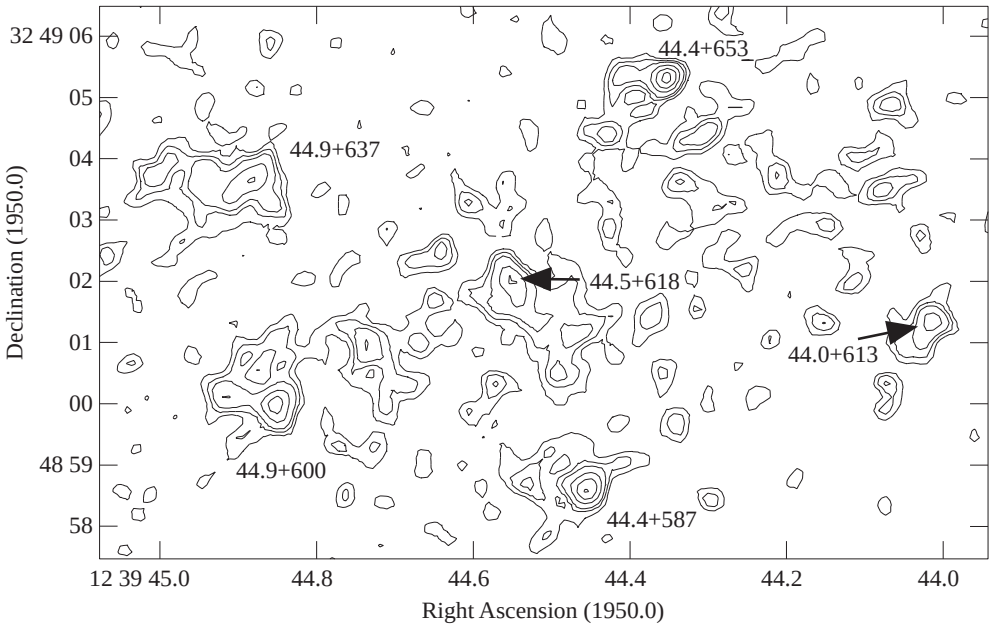

Fig. 4. Close-up view of CM67 at 4.86 GHz with the VLA A&B-array, contours are -3, 3, 4, 5, 7, 9, 11, 13, $15 \times 15\,\mu$Jy/beam

The advantage of having point source fluxes densities like that is that spectral indices can be determined despite the non-zero baselevel and missing spacing problems pertaining to interferometry data. Spectral indices α ($S_\nu \propto \nu^{-\alpha}$) were calculated from both the low and high resolution data pairs. Error estimates for the spectral index as listed in Table 3 were based on the assumption that the rms-noise in the maps is the typical error of the flux density determination. For weak sources with underlying diffuse emission larger errors may be introduced by erroneous fits of the point source fitting algorithm.

For several of the compact sources identified at subarcsecond resolution, low resolution flux densities were not determined because the larger beam would have picked up emission from neighbouring sources. Three sources, on the other hand, were included which were unresolved at 1.45″, but which were completely resolved out at $0.83 \times 0.61''$ resolution, so that the Gaussian fitting algorithm did not give useful results.

The sources were sorted into several categories according to their morphology at $0.46'' \times 0.44''$ resolution: point-like (p), marginally resolved (m), extended with no point source embedded (e), point source surrounded by significant extended emission even in the high resolution data (pe). For the latter two source types flux densities were difficult to determine since they sensitively depend on the fit area, i.e. how much of the extended emission around the source is used during the fit. We tried to use a fit area as small as possible. Yet, the significantly larger number of 'unphysical' (at least for the type of sources we expect to see), i.e. erroneous inverted 'p' and 'pe' spectra demonstrate that for the weaker of these sources the spectral index error estimates are too low.

Comparing the low and high resolution flux densities in the C-band we note that the low resolution values are always a factor of 1.5–4 larger. This indicates that the larger 1.45″ beam picked up extended emission around every source. Low and high resolution spectral indices are often different as well. Apart from the errors in the flux density determinations two effects can contribute to the discrepancies. (i) since the spectral indices were determined from different frequencies the high resolution values may be flatter due to a larger thermal fraction in the X band. (ii) spectral indices of a compact source and the surrounding extended emission, in particular for 'pe' and 'e' sources, may be different.

With these uncertainties in mind the spectral index information in Table 3 can only be used as a rough indicator of whether the radio emission has a thermal or synchrotron origin. We draw the following conclusions from this table.

(i) The spectral indices α of the bright source complex depicted in Fig. 2 are between 0.45 and 0.6, indicating non-thermal emission of all 4 components.
(ii) The middle of the central triple source (Fig. 3) has a flat spectral index (-0.22 ± 0.1), indicating either thermal emission or synchrotron self-absorption. The spectral indices of the two outer sources could be non-thermal ($\alpha \sim 0.3$), but the errors are large.
(iii) There are only two other point sources apart from the above-mentioned that are *likely* non-thermal: 40.1+578 and 44.4+653. There is one more point-source which may be both within the errors (44.0+613).
(iv) 41.7+611 and 42.0+620 may be non-thermal, but are extended and filamentary with no dominant point-sources embedded down to a flux density limit of 100 μJy.
(v) All the other spectral indices of sources are compatible with thermal emission.

4. Discussion

4.1. Emission distribution

The distribution of radio continuum emission in the central region of NGC 4631 is asymmetric with respect to the major and

minor axes, even when disregarding the bright western source which may be a background radio galaxy (cf. below). The north-south asymmetry with respect to the major axis may be caused by a highly non-axisymmetric distribution of thermal emission *in the disk* with most of the emission being on the far side of NGC 4631, or by emission truly bend out of the plane. Both can be a signature of gravitational interaction NGC4631 is undergoing.

We modeled the emission distribution with an open ring or torus of position angle of $81\pm1^\circ$, inclination $\sim 6.5^\circ$ and a radius of $\sim$1.8 kpc, with only the northern, distant half of the torus actually populated with radio sources. The ring is depicted in Fig. 1. It follows the observed emission distribution quite well, at least better than the major axis of the galaxy, and its center coincides with the nuclear triple source described above (Fig. 3). The radius of the ring would be similar to the radius of the inner star forming molecular gas disk. The difference of position angle and inclination to the values derived for the whole galaxy is small. Molecular rings are a common phenomenon in galaxies. Therefore we consider such a scenario as not unlikely. It remains open why only half of this torus would be populated with sources, i.e. shows star formation. If this is a common phenomenon other nearby starburst galaxies should be checked for similar emission distributions in their centers.

4.2. A tentative nucleus of NGC 4631?

In several spiral galaxies compact nuclear radio sources that are neither associated with a starburst nor with a supernova remnant have been found. M 81, for example, hosts a compact VLBI source (Bietenholz et al. 1996) interpreted as emission from a core intermediate in luminosity between a powerful AGN, and the relatively inactive core of the Galaxy. It shows Seyfert I characteristics (Filippenko & Sargent 1988). NGC 1068 is a classical example of a Seyfert 2 galaxy with a compact radio nucleus and jet (Muxlow et al. 1996) of similar origin. NGC 253, on the other hand, does not appear to be a Seyfert galaxy, but hosts a compact non-thermal core, plus an associated number of highly coaligned radio knots (Turner & Ho 1985).

NGC 4631 does not show Seyfert characteristics (Ho et al. 1995)[3]. However, the triple source in the center of our model ring is located almost within the estimated positional error circles of the stellar and dynamical centers (Fig. 3).

The monochromatic luminosity of the triple source in C–band (all three sources) is $\sim 5\cdot10^{24}$ erg s^{-1} Hz^{-1}, two orders of magnitude lower than the luminosity of the core of NGC 253 ($2\cdot10^{26}$ erg s^{-1} Hz^{-1} at 15 GHz, Turner & Ho 1985), and even lower than the core of M 81 ($2\cdot10^{27}$ erg s^{-1} Hz^{-1}, Bietenholz et al. 1996). The luminosity of SgrA*, on the other hand, is $1.1\cdot10^{23}$ erg s^{-1} Hz^{-1} (Backer 1994). Thus, if the triple source is located in the center of NGC 4631, it could be a mini-AGN intermediate in luminosity between the core of NGC 253, and the relatively quiescent core of the Galaxy.

4.3. Background radio galaxies

Alternatively, the triple source in the centre of NGC 4631 may be an external background radio galaxy. We found two other such radio galaxy candidates. One of them has been detected and resolved in our observation at RA=$12^{\rm h}\,39^{\rm m}\,26^{\rm s}$, DEC=$32^\circ43'\,37''$ (1950.0), but is outside the field of view discussed in this paper. The other one is the bright western-most non-thermal source complex. At $0.35''$ resolution the whole object is resolved into at least 3 components. The two outer ones may be identified with the lobes, and the central one with the core of the radio galaxy (cf. Fig. 2).

The two latter source complexes are likely radio galaxies because there is no alternative explanation. The occurrence of a third radio galaxy in the field would then not be too surprising. Unfortunately, optical identifications of the radio galaxies in the disk would be difficult, since they are outshined by the intense emission of HII region complexes. Only very high angular resolution ($< 0.1''$) radio data revealing clear morphological signatures for or against the case of a radio galaxy would finally resolve the issue of the origin of the triple source.

4.4. Nature of the central radio emission

Most of the compact or slightly extended radio sources in the central region of NGC4631 have flat spectral indices compatible with thermal emission both between L– and C–band, and C– and X–band (cf. Table 3). They can thus probably be attributed to HII-regions.

In Table 4 we compiled the average emission measures for the compact thermal sources. They are typically a factor 10–100 higher than the emission measures found in HII region complexes of most other nearby galaxies, in particular M31, M81, and NGC 6822, even though the linear resolution of those measurements was better (cf. Kennicutt 1984). NGC 4631's emission measures are comparable to those found in M101 and M33 derived at similar linear resolutions. Only the emission measures found in M82 are higher, and only by a factor of ~ 3. Thus the average emission measures (= surface brightnesses) in the central region of NGC 4631 on scales of 30–50 pc are among the highest found in nearby galaxies, and characteristic for a starburst.

The integrated radio continuum flux density of the central region (disregarding the contribution of the bright western radio galaxy) is 64 mJy in C-band B-array, and 85 mJy at L-band A-array. These values are uncorrected for missing large-scale emission, and comprise only 12% and 7%, resp., of the total flux densities of NGC 4631 as measured with single-dish telescopes (Hummel & Dettmar 1990). Since the uv-coverage of the C-band B-array data and the L-band A-array data is very similar we roughly see emission on the same scales, and a meaningful total spectral index between L– and C–band as measured with our data can be derived: 0.23 ($S_\nu \propto \nu^{-\alpha}$). Assuming a non-

[3] Recently, however, some evidence for mini Seyfert nuclei has been compiled in the literature (Maiolino & Rieke 1995; Ho et al. 1996). Such an object may easily be obscured by dust in the edge-on view of NGC 4631.

thermal spectral index of 0.8 (c.f. below) the thermal fraction then is 50% in C-band, much higher than the thermal fraction of ∼9% estimated from data including all the large-scale emission.

One can imply that the non-thermal emission is distributed on larger angular scales than the thermal emission, and is partly missed by the VLA A-array which lacks sensitivity on scales larger than 40″. The physical reason for the different distributions is that diffusion of cosmic rays along the mostly turbulent interstellar magnetic field tends to smear out the cosmic ray and thus the synchrotron emission distribution, whereas thermal emission is mostly closely associated with the hot young OB star population. Different scale lengths for synchrotron and thermal emission in galaxies were already pointed out by Bicay et al. (1989) and Bicay & Helou (1990). In NGC 4631, in particular, the difference in scale lengths should be large because of the extended synchrotron radio halo (Hummel & Dettmar 1990).

In spite of the high thermal fraction in our radio data there is almost no correlation of the radio emission with optical Hα data in the central region. Most of the thermal emission is heavily obscured at optical wavelengths. Our sensitivity for thermal radio emission at λ6cm in emission measure is 9×10^3 pc cm^{-6}. This is consistent with the non-detection of thermal radio emission in the outer disk, where Golla et al. (1996) found maximum emission measures of the order 10^3 pc cm^{-6} from optical data.

4.5. Thermal fraction and star formation rate

Several observational data constrain the possible thermal fraction of the total radio emission of NGC4631. They also constrain the star formation rate, if one assumes a certain initial mass function (IMF). We will use the extended Miller-Scalo IMF and give a high-mass (M $\gtrsim$ 10 M$_\odot$) SFR in the following.

(i) The Hα luminosity of NGC 4631 measured from optical data is $4.3^{+1.0}_{-0.8} \cdot 10^7$ L$_\odot$ (Golla et al. 1996). This luminosity is severely influenced by dust absorption and thus gives a lower limit to the thermal radio flux density and thermal fraction. Using the relation

$$\left(\frac{F_{therm}}{mJy}\right) = 2.238 \cdot 10^9 \left(\frac{T_e}{K}\right)^{0.42} \left(\frac{F_{H\alpha}}{erg\,s^{-1}\,cm^{-2}}\right) \times \left\{ ln(\frac{0.04995}{\nu[GHz]}) + 1.5 \cdot ln\left(\frac{T_e}{K}\right)\right\}^{-1}. \quad (1)$$

and $T_e = 10^4$ K we find F_{therm}= 23.7 mJy and f$_{th}$ = 4%. Sauvage & Thuan (1992) give a relation between the Hα luminosity and the star formation rate, yielding 0.23 M$_\odot$ yr^{-1} as a lower limit to the SFR in NGC4631.

(ii) In the above section we estimated the thermal fraction of the detected C-band emission to 50%. This would imply a thermal emission of 32 mJy in our C-band data. If one takes into account that we did not detect the thermal emission in the outer disk evident in the optical Hα data, and that the Hα and radio data are uncorrelated (Fig. 1), one may conclude that a reasonable estimate of the total thermal emission can be made by *adding* the contributions of radio and optical data. We then find F$_{therm}$ = 56 mJy and f$_{th}$ = 10%. The latter is in good agreement with the thermal fraction estimated from spectral fits to the total radio emission.

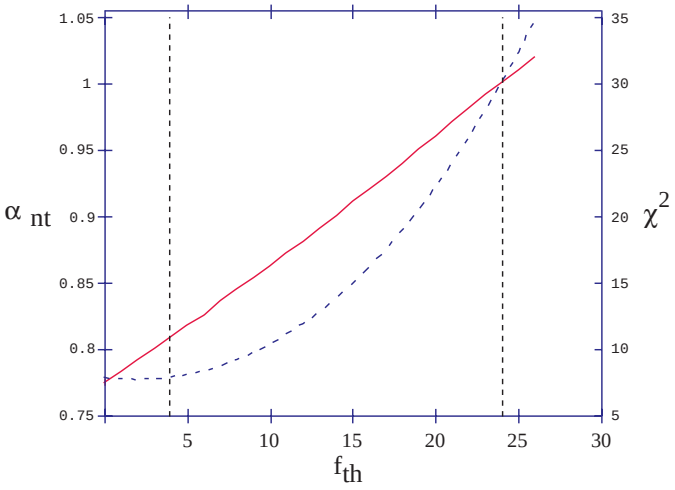

Fig. 5. Results of the fits to the total radio spectrum of NGC 4631 above 835 MHz. The hatched line represents χ^2 of the fits, whereas the straight line shows the non-thermal spectral index α_{nt} plotted against the thermal fraction f_{th}.

(iii) The FIR luminosity of NGC4631 taken from Rice et al. (1988) and converted to a distance of 7.5 Mpc is $9.1 \cdot 10^9$L$_\odot$. Using the relations given in Sauvage & Thuan (1992) we find a corresponding star formation rate of 1.3 M$_\odot$ yr^{-1}, a Hα luminosity of $2.4 \cdot 10^8$L$_\odot$, and a thermal fraction of 24%. These numbers are upper limits, because part of the FIR emission may come from dust heated by the general interstellar radiation field not associated with recent star formation (Devereux & Young 1990).

(iv) The total radio spectrum of NGC 4631 can be fitted with various combinations of non-thermal spectral indices α_{nt} and thermal fractions f_{th} in C-band. We used data from Hummel & Dettmar (1990) plus a more recent high frequency value at λ2.8 cm (265±12 mJy, Golla 1993) to compute χ^2 of the fits with thermal fractions in C-band from 0 to 26%. Fig. 5 depicts χ^2 and α_{nt} plotted against f_{th}. The fits yield a range of likely thermal fractions and non-thermal spectral indices. Thermal fractions above 15% in C-band are increasingly unlikely. A thermal fraction of 25% is three times less likely than a thermal fraction of 10%. It is thus likely that part of the detected FIR emission of NGC 4631 comes from dust heated by the general interstellar radiation field not associated with recent star formation (Devereux & Young 1990).

A range of plausible thermal fractions follows from the above considerations. f_{th} must be in the range 4% – 24%, and is likely to be between ∼8% and 15%. This also results in a range of plausible star formation rates for NGC4631, SFR $\sim 0.45 - 0.85$M$_\odot$ yr^{-1}. Our best estimate for the thermal fraction at C-band is $f_{th} \sim 10\%$, and for the star formation rate SFR ∼ 0.6 M$_\odot$ yr^{-1}.

Table 4. Properties of HII region complexes in the central region of NGC 4631

Source ID 1950.0	category	identification	low resolution emission measure [10^5 pc cm^{-6}]	low resolution n_e [cm^{-3}]	high resolution emission measure [10^5 pc cm^{-6}]	high resolution n_e [cm^{-3}]
38.0+519	m	OK	–	–	1.3	71
38.1+514	e	OK	1.0	44	2.0	87
39.5+563	pe	OK	0.86	40	1.2	68
41.0+603	e	OK	0.45	29	–	–
41.5+555	p	inv. syn.	–	–	1.5	76
41.7+611	e	?	1.0	44	–	–
42.0+619	e	?	0.76	38	–	–
44.0+613	e	?	0.32	25	–	–
44.4+587	pe	mixed?	0.52	31	1.3	71
44.5+617	e	OK	0.69	36	0.62	49
44.9+600	e	OK	0.57	33	0.95	60
44.9+637	e	OK	0.77	38	1.0	62

4.6. Star formation and supernova rates in NGC4631

Condon (1992) derived a supernova rate from the SFR of stars $M \gtrsim 5\,M_\odot$ using the "extended" Miller–Scalo IMF truncated at $M_{SN} = 100 M_\odot$. For this IMF the SFR we utilized above (for $M \gtrsim 10\,M_\odot$) is related to Condon's SFR by a factor 1.6, so that Condon's relation becomes

$$\left(\frac{\nu_{est}}{yr^{-1}}\right) \sim 0.066 \left[\frac{SFR(M \gtrsim 10 M_\odot)}{M_\odot\, yr^{-1}}\right]. \quad (2)$$

For NGC 4631 we find ν_{est} = 0.030–0.056 yr^{-1} for the above likely range of star formation rates.

2–3 of the radio point sources in our data (40.1+587, 44.4+653 and 44.4+587) are non-thermal and may thus originate from young supernova remnants. A crude estimate of their ages can be obtained from their luminosities assuming a power-law decay of the radio luminosity with time $\propto t^{-1.3}$ calibrated with CAS A. Using the relation given by van Buren & Greenhouse (1994; hereafter vBG) we find ages of 120, 240 & 275 yrs. We estimate that we did not detect any further radio-loud SNRs down to a flux limit (mainly given by confusion rather than the rms-noise) of 100 μJy at C-band. This limit corresponds to an age of $\sim$320 yrs. The SN rate can then be limited to 3 events within 320 yrs, or 0.009 yr^{-1}.

This is a factor of three to six less than ν_{est}. If NGC 4631 really had a radio supernova rate ν_{est}, we should have detected 9–18 young supernova remnants above our flux limit, i.e., younger than 320 yrs. If the star formation rate were $SFR_{FIR} = 1.3\,M_\odot$ yr^{-1}, we would even predict 25 young supernova remnants.

Several circumstances may have caused this discrepancy: (i) some of the flat-spectrum sources which we tentatively identified as HII–regions may actually be SNRs, (ii) SNRs in NGC 4631 on average have a lower maximum radio luminosity and/or a faster decrease in luminosity than CAS A, so that the assumptions of vBG are not valid, (iii) there are fewer supernova explosions in NGC 4631 than predicted by the "extended" Miller–Scalo IMF.

Table 5. NGC 4631 vs. M 82: supernova and star formation rates in comparison. ν_{est} is the supernova rate estimated from the SFRs. ν_{obs} was obtained with vBGs method. Data for L(IR) are from Rice et al. 1988, but see text; ν_{obs} of M 82 is from vBG.

	SFR	ν_{est}	ν_{obs}
NGC 4631	0.6 yr^{-1}$_{(est)}$	0.04 yr^{-1}	0.009 yr^{-1}
NGC 4631	1.3 yr^{-1}$_{(FIR)}$	0.08 yr^{-1}	0.009 yr^{-1}
M 82	2.0 yr^{-1}$_{(FIR)}$	0.13 yr^{-1}	0.12 yr^{-1}

It is our impression from the data that ill-identifications of SNRs as HII–regions could not make up for a factor of three to six, so that they cannot account for the whole discrepancy. Regarding (ii), it is difficult to access whether CAS A is a suitable 'standard' supernova remnant. Only very few young supernova remnants with accurately known ages are known.

Stars between 6 and 8 $M_\odot$ produce most of the supernovae, whereas stars more massive than $\sim 10 M_\odot$ produce most of the ionizing flux (Fig. 9 in Condon 1992). If there were indeed fewer supernova explosions in NGC 4631 than predicted by the "extended" Miller–Scalo IMF this would imply that the IMF of NGC 4631 is biased toward high-mass stars, or that it is flatter compared to the "extended" Miller–Scalo IMF.

Another galaxy where the IMF is often said to be biased towards high mass stars is M 82. Table 5 summarizes the star formation and supernova rates of NGC 4631 in comparison with M 82. In contrast to NGC 4631, the supernova rate of M 82 derived in vBG (ν_{obs}), as well as by other authors, and the rate estimated from the far-infrared luminosity (ν_{est}), *agree well* (cf. also Condon 1992). This may suggest that the IMF in M 82 is *not* biased towards high-mass stars. However, the good agreement for M 82 may well be a pure chance coincidence. Comparing M 82 and NGC 4631 directly, a valid statement is that in NGC 4631 either the average luminosities of SNRs are lower, or the IMF is indeed producing more high-mass stars than in M 82, or both.

A more reliable estimate of the number of young SNRs in NGC 4631 is required to put the 'biased-IMF' or 'low luminosity SNR' hypothesis on firmer grounds. Better angular resolution (≤ 10 pc) and sensitivity would permit us to differentiate more clearly SNRs from thermal emission, and to detect a suitable number of young SNRs to apply vBGs method with good statistics.

In addition, similar studies should be carried out for other galaxies. Studying the population of young supernova remnants at radio wavelengths, and comparing it with the star formation activity derived with various methods, may prove to be a powerful tool to investigate high mass star formation in starbursts.

Acknowledgements. G.G. was supported by the Alexander-von-Humboldt Stiftung with a Postdoctoral Fellowship at University of Toronto, and gratefully acknowledges advice and discussions with P.P. Kronberg during the course of this paper. Many thanks to the referee, J.J. Condon, who checked all the calculations, and found some significant bugs in the first version of this paper.

References

Aaronson M., 1978, PASP 90, 28 (Erratum 93, 535)
Antonucci R.R.J., Ulvestad J.S., 1988, ApJ 330, L97
Backer D.C., 1994, In: Zensus J.A., Kellermann K.I. (eds.) NRAO workshop No. 23, Compact Extragalactic Radio Sources. NRAO, Green Bank, p. 149
Bicay M.D., Helou G., Condon J.J., 1989, ApJ 338, L53
Bicay M.D., Helou G., 1990, ApJ 362, 59
Bietenholz M., Bartel N., Rupen M.P., et al., 1996, ApJ 457, 604
Briggs D.S., 1995, Ph.D. Thesis, The New Mexico Institute of Mining and Technology, Socorro, New Mexico
Condon J.J., 1992, ARA&A 30, 575
Devereux N.A., Joung J.S., 1990, ApJ 350, 25
Duric N., Dittmar M.R., 1988, ApJ 332, L67
Filippenko A.V., Sargent W.L.W., 1988, 324, 134
Golla G., 1993, Ph.D. Thesis, University of Bonn
Golla G., Dettmar R.-J., Domgörgen H., 1996, A&A 313, 439
Golla G., Hummel E., 1994, A&A 284, 777
Golla G., Wielebinski R., 1994, A&A 286, 733
Haslam C.G.T., Wilson W.E., Graham D.A., Hunt G.C., 1974, A&AS 13, 159
Ho L.C., Filippenko A.V., Sargent W.L.W., 1995, ApJS 98, 477
Ho L.C., Filippenko A.V., Sargent W.L.W., 1996, In: Peterson B.M., Cheng F.Z., Wilson A.S. (eds.) IAU Colloq. 159, Emission Lines in Active Galaxies: New Methods and Techniques. ASP, San Francisco
Hummel E., Dettmar R.-J., 1990, A&A 236, 23
Kennicutt R.C. Jr., 1984, ApJ 287, 116
Kronberg P.P., Biermann P., Schwab F.R., 1985, ApJ 291, 693
Kronberg P.P., Wilkinson P.N., 1975, ApJ 200, 430
Maiolino R., Rieke G.H., 1995, ApJ 454, 95
Muxlow T.W.B., Pedlar A., Wilkinson P.N., et al., 1994, MNRAS 266, 455
Muxlow T.W.B., Pedlar A., Holloway A.J., Gallimore J.F., Antonucci R.R.J., 1996, MNRAS 278, 854
Rice W., Lonsdale C.J., Soifer B.T., et al., 1988, ApJS 68, 91
Roy R.-J., Wang J., Arsenault R., 1991, AJ 101, 825
Saikia D.J., Unger S.W., Pedlar A., et al., 1990, MNRAS 245, 397
Sauvage M., Thuan T.X.T., 1992, ApJ 396, 269
Turner J.L., Ho P.T.P., 1985, ApJ 299, L77
van Buren D., Greenhouse M.A., 1994, ApJ 431, 640 (vBG)